

Efficiency enhancement in organic solar cells with ferroelectric polymers

Yongbo Yuan^{1,2}, Timothy J. Reece^{2,3}, Pankaj Sharma^{2,3}, Shashi Poddar^{2,3}, Stephen Ducharme^{2,3}, Alexei Gruverman^{2,3}, Yang Yang⁴ and Jinsong Huang^{1,2*}

The recombination of electrons and holes in semiconducting polymer–fullerene blends has been identified as a main cause of energy loss in organic photovoltaic devices. Generally, an external bias voltage is required to efficiently separate the electrons and holes and thus prevent their recombination. Here we show that a large, permanent, internal electric field can be ensured by incorporating a ferroelectric polymer layer into the device, which eliminates the need for an external bias. The electric field, of the order of $50 \text{ V } \mu\text{m}^{-1}$, potentially induced by the ferroelectric layer is tens of times larger than that achievable by the use of electrodes with different work functions. We show that ferroelectric polymer layers enhanced the efficiency of several types of organic photovoltaic device from 1–2% without layers to 4–5% with layers. These enhanced efficiencies are 10–20% higher than those achieved by other methods, such as morphology and electrode work-function optimization. The devices show the unique characteristics of ferroelectric photovoltaic devices with switchable diode polarity and tunable efficiency.

Polymeric organic photovoltaic (OPV) cells with polymer–fullerene bulk heterojunction are promising candidates for future low-cost, high-performance energy sources, owing to their low material and processing costs and mechanical flexibility^{1,2}. High efficiencies of 6–8% have been realized in polymeric OPVs by reducing both the optical bandgap and the highest occupied molecular orbital of the semiconducting polymers, and by optimizing the morphology of polymer–fullerene blend film with thermal annealing and solvent annealing^{3–9}. Although further optimization of the bandgap and highest occupied molecular orbital level of the semiconducting polymer is possible³, the path to increasing OPV efficiency to 15% must include recovery of significant energy loss even in the relatively high efficiency devices demonstrated so far^{10–12}. There are five main causes of reduced efficiency in OPV devices: energy level misalignment, insufficient light trapping and absorption, low exciton diffusion lengths, and non-radiative recombination of charges or charge-transfer excitons (CTEs), which consist of electrons at the acceptor and holes at the donor bound by Coulomb attraction, and low carrier mobilities^{11,13}. In many of the most efficient polymer–fullerene OPV devices, 50% or more of the energy loss is caused by the recombination of CTEs (ref. 11). For example, if we look at the most intensively studied material system, regioregular poly(3-hexylthiophene) (P3HT) and phenyl-C61-butyric acid methyl ester (PCBM) blend, the photocurrent at the maximum power output point is only 70% of what could be extracted by externally applying a large reverse bias voltage to the device¹⁴. The purpose of the present work is to show how to achieve greater efficiency using a large internal electrical field provided by the permanent electrical polarization of a ferroelectric (FE) polymer layer. To understand how this innovation works, we need to understand how internal electric fields affect charge extraction efficiency.

As illustrated in Fig. 1a, CTEs form right after the photoinduced electron transfer. The next step is to separate them and enable them to contribute to the photocurrent. CTEs can be treated as a precursors of free carriers, and their bandgap sets a maximum value for the open-circuit voltage (V_{oc} ; refs 10,15–23). The CTEs can be lost by non-radiative recombination when the dissociation driving forces (temperature and electric field) are small. The non-radiative recombination of CTEs, of course, reduces the photocurrent. In addition, the non-radiative recombination of CTEs reduces the free charge concentration, and then reduces the quasi-Fermi-energy (or chemical-potential) difference between electrons and holes, resulting in a lower V_{oc} , reducing the output power even further. A strong reduction of the non-radiative recombination is required to reduce the fundamental efficiency loss^{11,12,24}. Using the detailed balance theory, which was used to calculate the theoretical efficiency limit of a p–n junction solar cell in ref. 25, to treat a polymer–fullerene solar cell, a V_{oc} gain of 0.3–0.5 V by eliminating the non-radiative recombination pathways was predicted in ref. 13.

The mechanism of the non-radiative recombination of CTEs is not well understood^{13,24}. Nevertheless, there is a clear mechanism for dissociating the CTEs, and thus preventing recombination by applying a strong electric field to draw the electron and hole apart^{26–28}. The dissociation efficiency of CTEs into free charge carriers depends on the magnitude of the local electric field, where the probability of dissociation can be described quantitatively by the Onsager–Braun model²⁹. The probability (P) that a charge-transfer state is dissociated can be described by a field-dependent dissociation rate, k_D , and a field-independent decay rate, k_F , of the CTE (refs 26–28).

$$P(E) = \frac{k_D(E)}{k_D(E) + k_F} \quad (1)$$

¹Department of Mechanical Engineering, University of Nebraska-Lincoln, Lincoln, Nebraska 68588-0656, USA, ²Nebraska Center for Materials and Nanoscience, University of Nebraska-Lincoln, Lincoln, Nebraska 68583-0298, USA, ³Department of Physics and Astronomy, University of Nebraska-Lincoln, Lincoln, Nebraska 68588-0299, USA, ⁴Department of Materials Science and Engineering, University of California-Los Angeles, Los Angeles, California 90095-1595, USA. *e-mail: jhuang2@unl.edu.

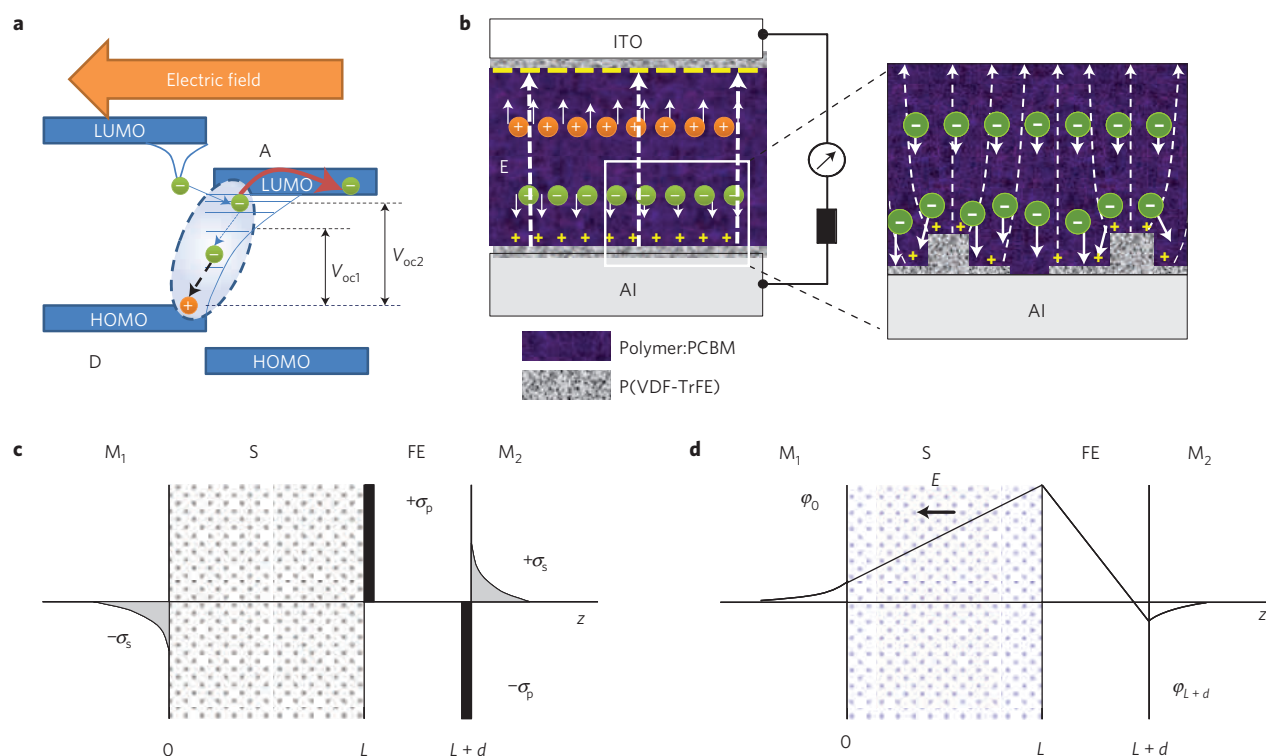


Figure 1 | Working principle of FE-OPV devices. **a**, Dynamic process for the dissociation of a (singlet) exciton to form a CTE (dashed oval) across the donor–acceptor interface, and the dissociation of the CTE to free carriers. Reduced CTE recombination results in a higher electron quasi-Fermi level and thus a higher V_{oc} . **b**, The structure of polymer photovoltaic devices with FE interfacial layers and a schematic diagram of electric field induced by the polarized FE layer and the field-assisted charge extraction. The right-hand panel illustrates the electric field distribution and electron conduction through the P(VDF-TrFE) on the Al side. **c, d**, Charge distribution and electrostatic potential profile of a junction with semiconductor (S) layer and ferroelectric (FE) layer inserted between two metal electrodes (M/S/FE/M) under the zero-bias condition. The surface charge density of the poled FE layer is σ_p . The induced screening charge density at the two electrodes is σ_s .

$k_D(E)$ is derived in ref. 28 to be

$$k_D(E) = k_R \frac{3}{4\pi a^3} e^{-E_b/kT} \left[1 + b + \frac{b^2}{3} + \frac{b^3}{18} + \frac{b^4}{180} + \dots \right] \quad (2)$$

where k_R is the bimolecular rate constant of the bound e–h pair, a is the initial separation of the bound e–h pair at the interface CTE, $b = e^3 E / 8\pi \epsilon_0 \epsilon_r k^2 T^2$, ϵ_0 is the dielectric permittivity of the vacuum, ϵ_r is the relative dielectric permittivity of the organic layer and E_b is the e–h pair’s binding energy. In most polymer–fullerene systems, a reverse bias larger than 5–10 V (electric field of 25–50 V μm^{-1} for 200-nm-thick film) is required to dissociate the majority of CTEs at room temperature²⁷. A small, internal electric field can be obtained even at zero device bias by using electrodes with different work functions. The electrode material used with conventional OPV devices, however, affords a work-function difference of no more than 2 V, producing an internal electric field of only 10 V μm^{-1} for typical device dimensions, which is much too small for efficient CTE dissociation³⁰. At the maximum-power point, the effective applied potential is even smaller, only 0.1–0.2 V (converted to 0.7 to 1.4 V μm^{-1} for a polymer thickness of 150 nm; refs 14,27). A new mechanism is then required to generate a ten-times-higher intrinsic electric field in the polymer semiconductor.

In this work, we incorporated the ultrathin FE film into polymer bulk heterojunction photovoltaic devices to increase efficiency with the induced polarization electric field. The device structure and working principle of the FE-OPV are shown in Fig. 1b. The ultrathin FE layer(s) were inserted at the interfaces of the organic semiconductor and metal electrodes. The two-dimensional FE materials have a net polarization electric field after poling. With

one type of charge partially or completely compensated by the metal electrode, the other type of charge sheet generates an electric field penetrating into the polymer semiconducting layer. The prerequisite for the operation of FE-OPV is the huge density of charges induced by FE polymer at the FE–semiconductor interface. These charges cannot be compensated by the low-concentration free charges in organic semiconductors, which leaves a large uncompensated internal field in the semiconductor. Vinylidene fluoride–trifluoroethylene copolymer, P(VDF-TrFE) (ref. 31), was the initial choice for the FE material for its advantages of chemical inertness, low fabrication temperatures, photostability and compatibility with polymer semiconducting materials. Its ferroelectricity originates from the molecular dipoles attached perpendicular to the chain axes and nearly normal to the plane of the thin film in the photovoltaic devices. A large electric polarization of the order of 100 mC m^{-2} can be produced with two-dimensional FE P(VDF-TrFE) films as thin as 1 nm (refs 32–35). The light-absorbing material used for most of this study was P3HT:PC₇₀BM. Another low-bandgap polymer, poly[(4, 4’-bis(2-ethylhexyl)dithieno[3,2-b:2’,3’-d]silole)-2,6-diyl-alt-(2,1,3-benzothiadiazole)-4,7-diyl] (PSBTBT) provided by Yang³⁶, was also briefly tested. The P(VDF-TrFE) thin film was deposited by Langmuir–Blodgett (LB) deposition or spin-coating^{32,37}. As P(VDF-TrFE) is a good insulator, the thickness of P(VDF-TrFE) was controlled well below 10 nm so that carriers could tunnel through it to electrodes.

The maximum electric field induced in the semiconductor layer by the FE polymer film was calculated with a simplified model of internal electric potential balance at zero device bias (short-circuit condition). The model of the charge distribution is constructed

by modifying the metal–FE–metal junction model of ref. 38 with a semiconductor layer inserted between the FE layer and one metal electrode. The charge distribution and respective electrostatic potential profile at short-circuit condition of a device with an FE layer inserted at the aluminium–semiconductor interface are plotted in Fig. 1c,d. A Thomas–Fermi model was used to describe the incomplete screening of the FE layer by the metal electrodes. The built-in electric field introduced by the P(VDF-TrFE) layer into the polymer is derived (see Supplementary Information for the derivation) to be

$$E = \frac{d\sigma_p}{\epsilon_0\epsilon_{FE}L} \quad (3)$$

where σ_p is the polarization charge density, d is the thickness of the P(VDF-TrFE) layer, L is the thickness of the polymer semiconductor layer and ϵ_{FE} is the relative dielectric constant of the P(VDF-TrFE) layer. The underlying physics is that the ultrathin FE layer has a large surface charge density that raises the electric static potential at the surface of the semiconductor layer. The FE polymer is assumed to uniformly cover the whole surface and be polarized in a direction nearly perpendicular to the plane. Using the nominal remnant polarization of 100 mC m^{-2} for P(VDF-TrFE), the electric field induced by the three monolayers (ML) (5 nm) P(VDF-TrFE) in a 150 nm P3HT:PC₇₀BM layer is calculated to be approximately $50 \text{ V } \mu\text{m}^{-1}$. Therefore, 3 ML of FE P(VDF-TrFE) can induce an electric field in the semiconductor layer that is sufficient to dissociate all the CTEs and suppress their non-radiative recombination. However, the actual induced electric field might be less than the model predicts owing to factors such as charge screening, possible incomplete poling of the FE layer and in particular the morphology of the FE layer, which will be shown below and in the supplementary document.

The influence of the induced electric field on the device performance is evident in the FE-OPV devices with P3HT:PC₇₀BM as the active layer, as shown in Fig. 2a. The addition of a 1 ML LB film of P(VDF-TrFE) led to a small increase in short-circuit current (I_{sc}), even before poling, probably owing to the partial poling of the P(VDF-TrFE) LB films that typically occurs during the deposition process⁴⁷, which is confirmed by the piezoresponse force microscopy (PFM) study to be shown later. After poling the FE layer by applying a large positive voltage pulse on the Al electrode, an extra electric field was added to the polymer–fullerene layer which had the same direction as the electric field induced by the electrode work-function difference. After positive poling, the I_{sc} increased from approximately 10 ± 1 to $12 \pm 1 \text{ mA cm}^{-2}$. There is a small variation in the maximum I_{sc} caused by the different P3HT:PC₇₀BM thicknesses used and the variation of remnant P(VDF-TrFE) polarization under different experimental conditions.

The electric field induced by the FE layer increases the V_{oc} of the OPV devices as well. The increase of the V_{oc} can be understood by considering the photovoltage loss mechanisms in OPV devices. First, the above-mentioned, field-assisted CTE dissociation process increases the photocurrent generation by reducing the recombination and, in the meantime, preserves the high quasi-Fermi energy of electrons, which then contributes to increasing the V_{oc} . In this scenario, the V_{oc} can be tuned continuously by controlling the electric field in the semiconductor, which has been realized by a partial polarization of P(VDF-TrFE) in our devices (Supplementary Fig. S2). Second, the voltage loss in photovoltaic devices is also related to the saturated dark current of the device^{13,39,40}. The poled FE polymer film was found to reduce the saturated dark current by two orders of magnitude, as shown in Fig. 2b. The reduced saturated dark current should be ascribed to a high carrier-injection barrier at reverse bias introduced by the FE dipole layer. The poled FE polymer film also controls the dark

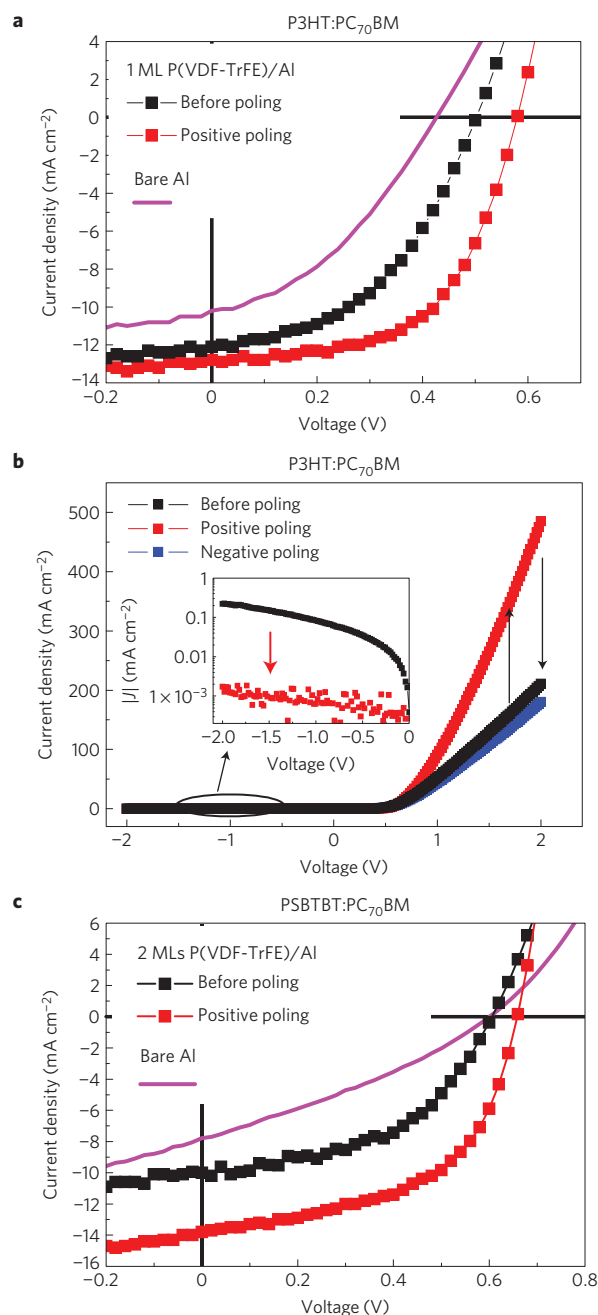


Figure 2 | Improvement in device performance by the FE layer. The control devices have the structure of ITO/PEDOT:PSS/polymer:PC₇₀BM/Al, and the FE-OPVs have the FE layer inserted at the polymer/Al interfaces.

a, Photocurrents of P3HT:PC₇₀BM devices without an FE layer (magenta line) and with an FE layer before poling (black squares), and with an FE layer after positive poling (red squares). **b**, Dark current of devices with 1 ML P(VDF-TrFE) film before and after positive and negative poling; the inset compares the reverse saturated dark currents of a device before and after positive poling. **c**, Photocurrent of a PSBTBT:PC₇₀BM device without an FE layer (magenta line), with an FE layer before poling (black square line) and with an FE layer after poling (red squares).

current of the device. The energy efficiency is increased from 1.7% to 4.5% after positive poling.

In addition to the greater free-carrier generation by the increased geminate-pair separation, the induced electric field is also expected to increase the photogenerated-carrier collection by increasing the drift length of the carriers and/or extend the charge

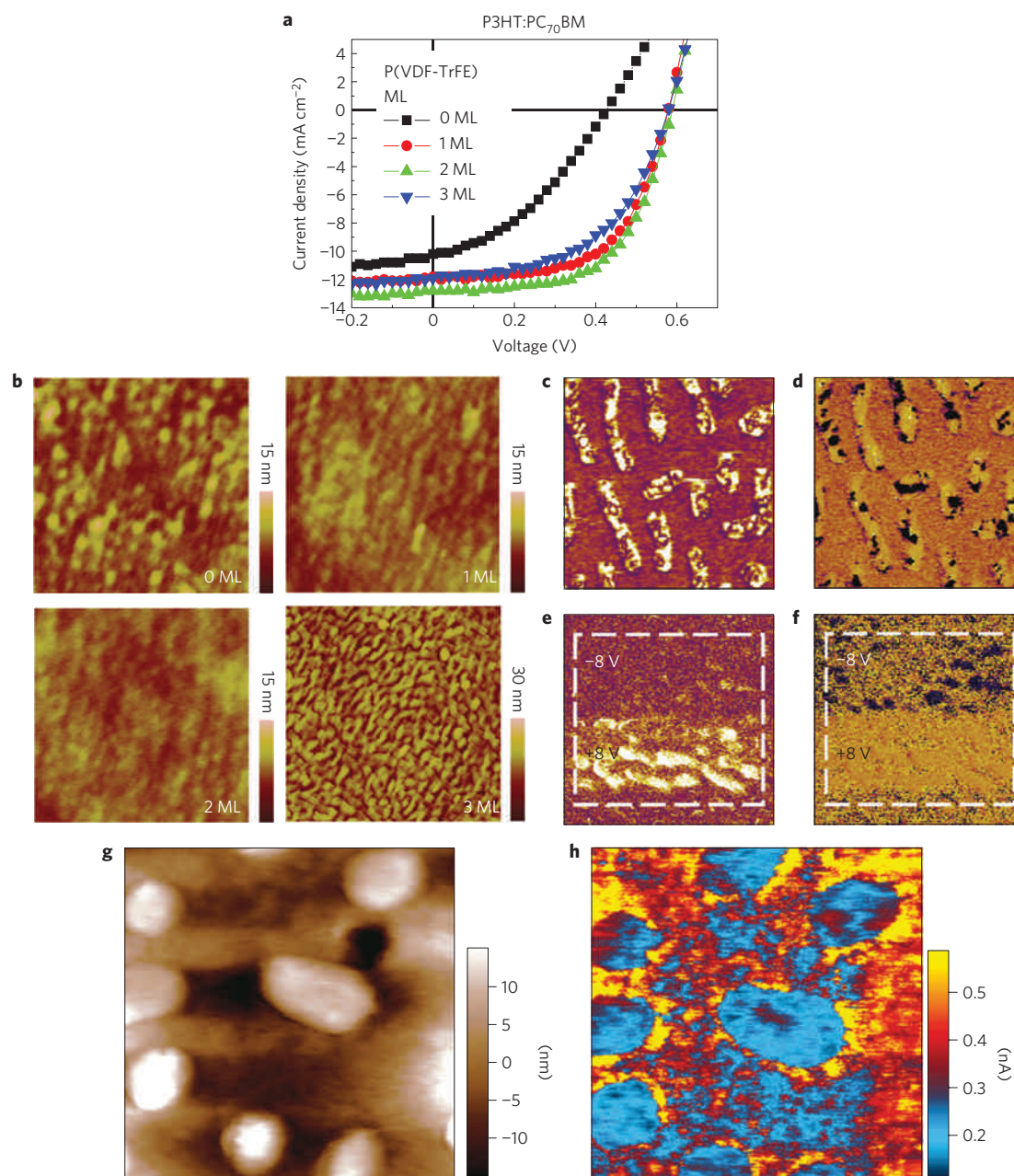


Figure 3 | Morphologies of FE films and their effect on the device performance. **a**, Comparison of the I - V curves of P3HT:PC₇₀BM devices with 0–3 ML P(VDF-TrFE) at the cathode interface. **b**, Surface morphology of P3HT:PCBM film covered by 0–3 ML of P(VDF-TrFE) tested by AFM in tapping mode ($4\ \mu\text{m} \times 4\ \mu\text{m}$). **c,d**, PFM amplitude and phase image of a 2 ML P(VDF-TrFE) layer on a P3HT:PCBM film, tested by PFM in contact mode ($1\ \mu\text{m} \times 1\ \mu\text{m}$) with Pt/Ti-coated silicon tips. **e,f**, PFM amplitude and phase image of a 2 ML P(VDF-TrFE) layer on a P3HT:PCBM top, poled by $\pm 8\ \text{V}$ d.c. bias with a PFM tip under contact mode ($1\ \mu\text{m} \times 1\ \mu\text{m}$). **g,h**, AFM topography and conducting AFM current mapping of the same area ($500\ \text{nm} \times 500\ \text{nm}$) of a P3HT:PCBM film covered with 2 ML P(VDF-TrFE).

bimolecular-recombination lifetime. The carrier drift length is the product of carrier mobility, carrier recombination lifetime and internal electric field. Such a mechanism is especially important to semiconductor polymers with low carrier mobility, where a thicker layer can be used to increase the light absorption efficiency of OPV devices without sacrificing carrier collection efficiency. This was confirmed in our test of the low-bandgap material PSBTBT, which has a carrier mobility an order of magnitude lower than that of P3HT (ref. 7). It was found that a thicker (90 nm) film is needed to reach the optimized efficiency in the device with an FE layer than in a regular device (80 nm). The efficiency of the device with a PSBTBT:PC₇₀BM active layer was increased from 1.5% to 4.9%

by inserting 2 ML P(VDF-TrFE) and poling (Fig. 3c; ref. 41). The devices with the Al cathode instead of calcium (Ca) were used as control devices because Ca chemically reacts with P(VDF-TrFE) and kills the ferroelectricity of P(VDF-TrFE). Nevertheless, all the FE-OPVs have already shown higher efficiencies than optimized devices with Ca as the cathode (see Table 1; refs 42,43).

According to equation (3), a thicker P(VDF-TrFE) layer can introduce a larger electric field into the semiconductor layer. However, the increased P(VDF-TrFE) layer thickness also increases the contact resistance, which would reduce device efficiency. This was studied in our experiments by increasing the thickness of P(VDF-TrFE) from 0 ML to 3 ML. The current–voltage (I - V)

Table 1 | Comparing the device performance with 0–3 ML FE materials.

Anode	Semiconducting layer	Cathode	J_{sc} (mA cm ⁻²)	V_{oc} (V)	FF (%)	PCE (%)
MoO ₃ /Ag	P3HT:PC ₆₀ BM	Bare ITO	6.41	0.183	31	0.37
		1 ML LB film/ITO	7.60	0.405	41	1.3
		2 ML LB film/ITO	7.49	0.460	49	1.7
		3 ML LB film/ITO	6.65	0.418	46	1.3
ITO/PEDOT:PSS	P3HT:PC ₇₀ BM	Bare Al	10.2	0.426	38	1.7
		Ca/Al	10.5	0.582	61	3.7
		1 ML LB film/Al	11.8	0.579	60	4.1
		2 ML LB film/Al	12.8	0.589	60	4.5
		3 ML LB film/Al	11.9	0.579	52	3.6
		3 ML LB film/Al	13.1	0.654	54	4.6
ITO/PEDOT:PSS	PSBTBT:PC ₇₀ BM	Bare Al	7.78	0.600	31	1.5
		Ca/Al	13.2	0.660	51	4.4
		1 ML LB film/Al	12.1	0.647	53	4.2
		2 ML LB film/Al	13.8	0.660	54	4.9
		3 ML LB film/Al	13.1	0.654	54	4.6
		3 ML LB film/Al	13.1	0.654	54	4.6

characteristics of the P3HT:PC₇₀BM devices with 0–3 ML of P(VDF-TrFE) after poling are shown in Fig. 3a. One or two monolayers of P(VDF-TrFE) was the optimum thickness range for P3HT:PC₇₀BM. From this point of view, the absence of a critical thickness for the ferroelectricity of two-dimensional P(VDF-TrFE) is crucial to ensuring that the FE-OPV can work so well. An increased thickness to three monolayers of P(VDF-TrFE) resulted in slightly reduced efficiency for P3HT:PCBM devices, although it is still much larger than the device without an FE layer. To understand the device performance variation with P(VDF-TrFE) thickness, we studied the morphology of P(VDF-TrFE) by atomic force microscopy (AFM), as shown in Fig. 3b. The pristine P(VDF-TrFE) LB films are continuous before annealing but become non-continuous and rougher after thermal annealing. The roughness data, ranging from 0.8 nm to 1.7 nm for films before annealing, and from 1.0 nm to 3.6 nm after annealing, are summarized in Supplementary Table S1. It is clearly shown that the 3 ML films of P(VDF-TrFE) aggregate after annealing, forming many nanomesas. This must be caused by the mismatch of surface energy between the P3HT:PCBM film and P(VDF-TrFE) film, and the formation of nanomesas helps to minimize the surface energy⁴⁴. The thickness of the nanomesas formed by annealing 3 ML of P(VDF-TrFE) is approximately 10 nm (Supplementary Fig. S3), which is too thick for efficient tunnelling of electrons through this layer, and explains the reduced photocurrent. The highest efficiency occurs at a balance of electric fields added by the P(VDF-TrFE) layers and the series resistance introduced by the insulating P(VDF-TrFE) layers.

The 1–2 ML of P(VDF-TrFE) film were also found to be non-continuous, with P(VDF-TrFE) islands sitting on P3HT:PCBM, from the PFM measurement (Fig. 3c,d). The spontaneous polarization of P(VDF-TrFE) on P3HT:PCBM exhibits a preferred direction and the same direction as positively poled P(VDF-TrFE), which explains the observed increased photocurrent in the devices with P(VDF-TrFE) layers even before positive poling. The detailed mechanism of the initial net polarization is still not clear but is believed to be related to the difference in chemical affinity of F and H to the substrates or semiconducting polymer⁴⁵. The P(VDF-TrFE) films on P3HT:PCBM were directly poled by the PFM tip with an applied voltage of ± 8 V and the polarization imaged by PFM (Fig. 3e,f), which confirmed the ultrathin P(VDF-TrFE) film's ferroelectricity at the nanoscale. After poling, the electric fields from all FE film areas point in the same direction.

To understand how the current conducts through the ultrathin insulating FE films, their conductance was measured at nanoscale with conducting AFM in conjunction with PFM on

the same area (500 nm \times 500 nm) of 2 ML P(VDF-TrFE)-covered P3HT:PCBM/poly(3,4-ethylenedioxythiophene):polystyrenesulphonate (PEDOT:PSS)/indium tin oxide (ITO) under small bias. The conductance of the P(VDF-TrFE) can be well correlated to the thickness and morphology. It is clear that the current is smaller through the nanomesa than through the area surrounding the nanomesa unless at FE domain boundaries. It is evident in Fig. 3e,f that there is still a very thin layer of P(VDF-TrFE) surrounding the nanomesas whose thickness might be in the range of tunnelling length. The thickness of this remaining layer was not determined because of the large roughness of the semiconducting polymer film. The charges can go through these thin P(VDF-TrFE) layers although the electric field in P(VDF-TrFE) is in the opposite direction. It is believed that the thicker FE nanomesas mainly contribute a large induced electric field in the semiconductor polymer on the top of and around them and increase the average induced electric field, but thinner FE surrounding layers are more efficient in collecting charges. This result also implies the potential to further increase the FE-OPV efficiency by optimizing the morphology of FE polymer such as the thickness and the area ratio of thick and thin FE polymer islands.

The non-continuous P(VDF-TrFE) nanomesas covered less than 50% of the surface of P3HT:PCBM film, as inferred from Fig. 3c,d. The incomplete coverage inevitably leads to a smaller, induced internal electric field than calculated by equation (3). The actual electric field produced by the FE layer was calculated by extrapolating the photocurrent of the device without P(VDF-TrFE) at reverse bias (Supplementary Fig. S4). Here we used the assumption that the photocurrent is only determined by the effective electric field applied²⁷. The enhanced I_{sc} in FE-OPV compared with the regular OPV is attributed to the electric field added by the FE layer. The extracted electric field due to the FE polymer was approximately 12 ± 3 V μm^{-1} added by P(VDF-TrFE), which is much less than the calculated result of 50 V μm^{-1} . There is therefore plenty of room for improvement, which was verified by the observation that application of a large reverse bias of -5 V produced an even larger photocurrent of 15 mA cm⁻² (compared with 10 mA cm⁻² at the maximum-power point) in the P3HT:PC₇₀BM device.

The FE-OPV shows the unique characteristics of an FE photovoltaic with switchable diode polarity and tunable device efficiencies. As shown in Fig. 4, the polarity of the device with 1 ML P(VDF-TrFE) inserted at both anode and cathode can be completely switched by the ± 15 V pulse. The current of the pristine device shows nearly Ohmic behaviour and little rectification. The I - V curve becomes asymmetric with a much

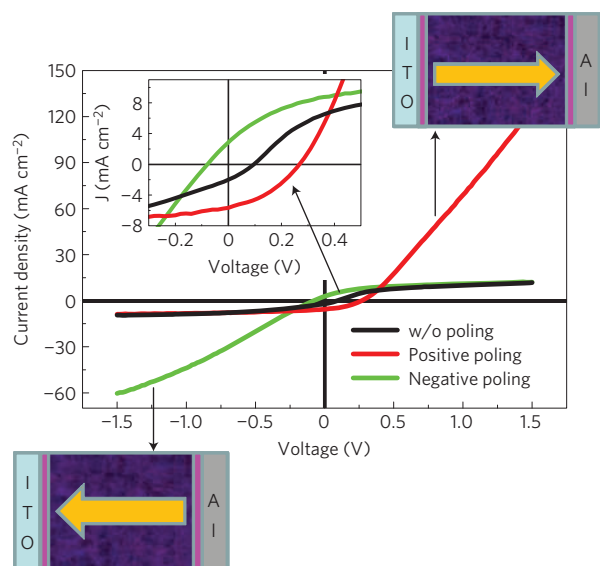


Figure 4 | Switch behaviours of FE-OPV devices. Photocurrent output from a device with a structure of ITO/1 ML P(VDF-TrFE)/P3HT:PCBM/1 ML P(VDF-TrFE)/Al. The inset zooms in the I - V curves around zero bias.

larger rectification with diode characteristics after positive poling or negative poling. This is the first time that both a switchable diode and photovoltaic devices have been demonstrated. The larger V_{oc} in the positively poled devices is consistent with the fact that there is a built-in electric field pointing from Al to ITO as well as an asymmetric polarization of P(VDF-TrFE) due to the interface chemistry effect⁴⁶. The devices with an FE layer inserted at the cathode interface, either the Al cathode or the ITO cathode, also show a switchable photocurrent alternating between high-efficiency and low-efficiency states as the FE film polarization is switched back and forth by positive and negative voltage pulses (see Supplementary Figs S5 and S7). This result also demonstrates that P(VDF-TrFE) can be used as a universal interface material for electrodes, greatly expanding the design and fabrication flexibility. The switchable nature of the photocurrent and photovoltage by poling P(VDF-TrFE) along the two opposite directions implies that the FE polarization has a dominant role in the observed photovoltaic enhancement effect. The efficiency of our FE-OPV is several orders of magnitude larger than the largest reported efficiency of other FE photovoltaic devices⁴⁷.

In summary, we report an FE-OPV hybrid device, which has both FE photovoltaic and OPV characteristics. The electric field induced by the ultrathin FE polymer films significantly increased the device efficiency, from 1–2% without the FE film to 4–5% after poling the FE layer. These enhanced efficiencies are 10–20% higher than those achieved by other methods, such as morphology and electrode work-function optimization. There is still ample opportunity to further increase the efficiency of the FE-OPV devices with our current semiconducting polymers by using a better-controlled morphology and thickness of the FE film. The theoretical limit of I_{sc} from FE-OPV can be derived from the photocurrent of regular OPV at a reverse bias of -10 V. With the increased electric field to eliminate the CTEs' recombination and bimolecular recombination⁴⁸, a further increase of V_{oc} is expected¹³. Also note that the increase of V_{oc} may not be as pronounced as the optimum 0.3–0.5 V because there may be modes of non-radiative charge recombination that are field independent, such as defect- or impurity-mediated charge recombination. The increased V_{oc} can also be partially offset by the contact resistance brought by the insulating FE layer.

Further work is necessary to optimize the morphology of the FE film to take full advantage of its electric field and increase charge-collection efficiencies, while ensuring efficient transfer to the electrodes with minimum conduction resistance through the FE film.

Methods

For the device fabrication, PEDOT:PSS (Baytron-P 4083) was first spin-cast onto a cleaned ITO/glass substrate at a spin speed of 3,500 r.p.m., which gives a PEDOT:PSS film thickness of approximately 30 nm, as measured with a Dektak profilometer. The spun PEDOT:PSS was then baked at 120 °C for 20 min before spin-casting the polymer film. P3HT (purchased from Rieke Metals, used as received) was first dissolved in 1,2-dichlorobenzene to make 30 mg ml⁻¹ solution, followed by blending with PC₇₀BM (purchased from Nano-C, used as received) in a ratio of 1:1 by weight. The blend was stirred for about 14 h at 40 °C in a nitrogen-filled glove box. The active layer was obtained by spin-coating the blend at 800 r.p.m. for 20 s, and the thickness of the P3HT:PC₇₀BM film is approximately 150 nm. For the devices based on PSBTBT, both PSBTBT and PC₇₀BM were dissolved in chlorobenzene in a 1.5:1 (10 mg ml⁻¹) ratio. The film was obtained by spin-coating at 2,000 r.p.m., then annealed at 140 °C for 5 min, and the thickness of the film was approximately 90 nm.

The LB deposition, although not the only choice for the deposition of P(VDF-TrFE) onto polymer semiconductor or ITO, has the unique capability to form a conformal and controlled ultrathin film to the level of 1 ML and has more tolerance to surfaces with different surface energies⁴⁷. For the deposition of FE LB films, the random copolymer P(VDF-TrFE), containing 70% vinylidene fluoride and 30% trifluoroethylene, was dissolved in dimethyl sulphoxide with a concentration of 0.05% by weight. The polymer was dispersed on the surface of ultrapure (18 MΩ cm) water, and slowly compressed to a surface pressure of 5 mN m⁻¹ at room temperature in air. Then the LB layer was transferred to a glass/ITO substrate covered with P3HT:PC₇₀BM or PSBTBT:PC₇₀BM film. The P(VDF-TrFE) films were deposited 1 ML at a time by horizontal dipping. The samples were annealed at 135 °C in N₂ for half an hour to improve the crystallinity of the P(VDF-TrFE; ref. 30). The FE LB film preparation procedure is described in detail in ref. 48.

The active device area was 0.08 cm². Photocurrent measurement was done under simulated air mass 1.5 global irradiation (100 mW cm⁻²) using a xenon-lamp-based solar simulator (Oriel 67005, 150 W Solar Simulator). A Schott visible-colour glass-filtered (KG5 colour-filtered) Si diode (Hamamatsu S1133) was used to calibrate the light intensity before photocurrent measurement.

Received 7 June 2010; accepted 23 December 2010;
published online 13 February 2011

References

- Yu, G., Gao, J., Hummelen, J. C., Wudl, F. & Heeger, A. J. Polymer photovoltaic cells: Enhanced efficiencies via a network of internal donor-acceptor heterojunctions. *Science* **270**, 1789–1791 (1995).
- Sariciftci, N. S., Smilowitz, L., Heeger, A. J. & Wudl, F. Photoinduced electron transfer from a conducting polymer to buckminsterfullerene. *Science* **258**, 1474–1476 (1992).
- Chen, H. Y. *et al.* Polymer solar cells with enhanced open-circuit voltage and efficiency. *Nature Photon.* **3**, 649–653 (2009).
- Park, S. H. *et al.* Bulk heterojunction solar cells with internal quantum efficiency approaching 100%. *Nature Photon.* **3**, 297–303 (2009).
- Liang, Y. *et al.* For the bright future—bulk heterojunction polymer solar cells with power conversion efficiency of 7.4%. *Adv. Mater.* **22**, 1–4 (2010).
- Kim, J. Y. *et al.* Efficient tandem polymer solar cells fabricated by all-solution processing. *Science* **317**, 222–225 (2007).
- Chen, H.-Y. *et al.* Silicon atom substitution enhances interchain packing in a thiophene-based polymer system. *Adv. Mater.* **21**, 1–5 (2009).
- Liang, Y. Y. *et al.* Development of new semiconducting polymers for high performance solar cells. *J. Am. Chem. Soc.* **131**, 56–57 (2009).
- Liang, Y. Y. *et al.* Highly efficient solar cell polymers developed via fine-tuning of structural and electronic properties. *J. Am. Chem. Soc.* **131**, 7792–7799 (2009).
- Veldman, D., Meskers, S. C. J. & Janssen, R. A. J. The energy of charge-transfer states in electron donor-acceptor blends: Insight into the energy losses in organic solar cells. *Adv. Funct. Mater.* **19**, 1939–1948 (2009).
- Kirchartz, T., Taretto, K. & Rau, U. Efficiency limits of organic bulk heterojunction solar cells. *J. Phys. Chem. C* **113**, 17958–17966 (2009).
- Veldman, D. *et al.* Compositional and electric field dependence of the dissociation of charge transfer excitons in alternating polyfluorene copolymer/fullerene blends. *J. Am. Chem. Soc.* **130**, 7721–7735 (2008).
- Vandewal, K., Tvingstedt, K., Gadisa, A., Inganäs, O. & Manca, J. V. On the origin of the open-circuit voltage of polymer-fullerene solar cells. *Nature Mater.* **8**, 904–909 (2009).

14. Shrotriya, V., Yao, Y., Li, G. & Yang, Y. Effect of self-organization in polymer/fullerene bulk heterojunctions on solar cell performance. *Appl. Phys. Lett.* **89**, 063505 (2006).
15. Brabec, C. J. *et al.* Origin of the open circuit voltage of plastic solar cells. *Adv. Funct. Mater.* **11**, 374–380 (2001).
16. Gadisa, A., Svensson, M., Andersson, M. R. & Inganäs, O. Correlation between oxidation potential and open-circuit voltage of composite solar cells based on blends of polythiophenes/fullerene derivative. *Appl. Phys. Lett.* **84**, 1609–1611 (2004).
17. Cravino, A. Origin of the open circuit voltage of donor–acceptor solar cells: Do polaronic energy levels play a role? *Appl. Phys. Lett.* **91**, 243502 (2007).
18. Cremer, J., Bauerle, P., Wienk, M. M. & Janssen, R. A. J. High open-circuit voltage poly(ethynylene bithienylene): Fullerene solar cells. *Chem. Mater.* **18**, 5832–5834 (2006).
19. Roquet, S. *et al.* Triphenylamine–thienylenevinylene hybrid systems with internal charge transfer as donor materials for heterojunction solar cells. *J. Am. Chem. Soc.* **128**, 3459–3466 (2006).
20. Mutolo, K. L., Mayo, E. I., Rand, B. P., Forrest, S. R. & Thompson, M. E. Enhanced open-circuit voltage in subphthalocyanine/C-60 organic photovoltaic cells. *J. Am. Chem. Soc.* **128**, 8108–8109 (2006).
21. Scharber, M. C. *et al.* Design rules for donors in bulk-heterojunction solar cells—towards 10% energy-conversion efficiency. *Adv. Mater.* **18**, 789–794 (2006).
22. Rand, B. P., Burk, D. P. & Forrest, S. R. Offset energies at organic semiconductor heterojunctions and their influence on the open-circuit voltage of thin-film solar cells. *Phys. Rev. B* **75**, 115327–115337 (2007).
23. Schueppel, R. *et al.* Optimizing organic photovoltaics using tailored heterojunctions: A photoinduced absorption study of oligothiophenes with low band gaps. *Phys. Rev. B* **77**, 085311–085324 (2008).
24. Tvingstedt, K. *et al.* Electroluminescence from charge transfer states in polymer solar cells. *J. Am. Chem. Soc.* **131**, 11819–11824 (2009).
25. Shockley, W. & Queisser, H. Detailed balance limit of efficiency of p–n junction solar cells. *J. Appl. Phys.* **32**, 510–519 (1961).
26. Veldman, D. *et al.* Compositional and electric field dependence of the dissociation of charge transfer excitons in alternating polyfluorene copolymer/fullerene blends. *J. Am. Chem. Soc.* **130**, 7721–7735 (2008).
27. Mihailetchi, V. D., Koster, L. J. A., Hummelen, J. C. & Blom, P. W. M. Photocurrent generation in polymer–fullerene bulk heterojunctions. *Phys. Rev. Lett.* **93**, 216601–216604 (2004).
28. Braun, C. L. Electric field assisted dissociation of charge transfer states as a mechanism of photocarrier production. *J. Chem. Phys.* **80**, 4157–4161 (1984).
29. Onsager, L. Deviations from ohm's law in weak electrolytes. *J. Chem. Phys.* **2**, 599–615 (1934).
30. Kim, J. Y. *et al.* New architecture for high-efficiency polymer photovoltaic cells using solution-based titanium oxide as an optical spacer. *Adv. Mater.* **18**, 572–576 (2006).
31. Furukawa, T. Ferroelectric properties of vinylidene fluoride copolymers. *Phase Transit.* **18**, 143–211 (1989).
32. Bune, A. V. *et al.* Two-dimensional ferroelectric films. *Nature* **391**, 874–877 (1998).
33. Ducharme, S., Palto, S. P., Blinov, L. M. & Fridkin, V. M. Physics of two-dimensional ferroelectric polymers. *AIP Conf. Proc.* **535**, 354–363 (2000).
34. Junquera, J. & Ghosez, P. Critical thickness for ferroelectricity in perovskite ultrathin films. *Nature* **422**, 506–509 (2003).
35. Ahn, C. H., Rabe, K. M. & Triscone, J. M. Ferroelectricity at the nanoscale: Local polarization in oxide thin films and heterostructures. *Science* **303**, 488–491 (2004).
36. Hou, J. H., Chen, H. Y., Zhang, S. Q., Li, G. & Yang, Y. Synthesis, characterization, and photovoltaic properties of a low band gap polymer based on silole-containing polythiophenes and 2,1,3-benzothiadiazole. *J. Am. Chem. Soc.* **130**, 16144–16145 (2008).
37. Sorokin, A. V., Bai, M., Ducharme, S. & Poulsen, M. Langmuir–Blodgett films of polyethylene. *J. Appl. Phys.* **92**, 5977–5981 (2002).
38. Zhuravlev, M. Y., Sabirianov, R. F., Jaswal, S. S. & Tsymbal, E. Y. Giant electroresistance in ferroelectric tunnel junctions. *Phys. Rev. Lett.* **94**, 246802 (2005).
39. Li, N., Lassiter, B. E., Lunt, R. R., Wei, G. & Forrest, S. R. Open circuit voltage enhancement due to reduced dark current in small molecule photovoltaic cells. *Appl. Phys. Lett.* **94**, 023307 (2009).
40. Potsavage, W. J., Yoo, S. & Kippelen, B. Origin of the open-circuit voltage in multilayer heterojunction organic solar cells. *Appl. Phys. Lett.* **93**, 193308 (2008).
41. Liang, Y. *et al.* Development of new semiconducting polymers for high performance solar cells. *J. Am. Chem. Soc.* **131**, 56–57 (2008).
42. Sista, S., Hong, Z. R., Park, M. H., Xu, Z. & Yang, Y. High-efficiency polymer tandem solar cells with three-terminal structure. *Adv. Mater.* **22**, E77–E80 (2010).
43. Sista, S. *et al.* Highly efficient tandem polymer photovoltaic cells. *Adv. Mater.* **22**, 380–383 (2010).
44. Bai, M. J. & Ducharme, S. Ferroelectric nanomesa formation from polymer Langmuir–Blodgett films. *Appl. Phys. Lett.* **85**, 3528–3530 (2004).
45. Duan, C. G., Sabirianov, R. F., Mei, W. N., Jaswal, S. S. & Tsymbal, E. Y. Interface effect on ferroelectricity at the nanoscale. *Nano Lett.* **6**, 483–487 (2006).
46. Chen, X. Q., Yamada, H., Horiuchi, T. & Matsushige, K. Investigation of surface potential of ferroelectric organic molecules by scanning probe microscopy. *Jpn. J. Appl. Phys. Part 1* **38**, 3932–3935 (1999).
47. Qin, M., Yao, K. & Liang, Y. C. High efficient photovoltaics in nanoscaled ferroelectric thin films. *Appl. Phys. Lett.* **93**, 122904 (2008).
48. Ducharme, S., Palto, S. P. & Fridkin, V. M. in *Ferroelectric and Dielectric Thin Films* (ed. Nalwa, H. S.) 545–591 (Academic, 2002).

Acknowledgements

S.D. thanks the Nebraska Research Initiative and the National Science Foundation Materials Research Science and Engineering Center for financial support (DMR-0820521). A.G. acknowledges financial support from the US Department of Energy, Office of Basic Energy Sciences, Division of Materials Sciences and Engineering under award DE-SC0004530.

Author contributions

J.H. conceived the idea. J.H. and Y. Yuan designed the experiments. Y. Yuan carried out the fabrication of photovoltaic devices, the current–voltage measurement, the AFM and electrostatic force microscopy measurements and data analysis. Y. Yuan constructed the model. T.J.R., S.P. and S.D. carried out the deposition of P(VDF-TrFE) LB film and capacitance measurement. P.S. and A.G. were responsible for the PFM and conducting AFM measurement. Y. Yang provided the PSBTBT polymer. Y. Yuan, J.H., T.J.R. and S.D. analysed the data. J.H. and Y. Yuan wrote the paper. S.D. reviewed and commented on the paper.

Additional information

The authors declare no competing financial interests. Supplementary information accompanies this paper on www.nature.com/naturematerials. Reprints and permissions information is available online at <http://npg.nature.com/reprintsandpermissions>. Correspondence and requests for materials should be addressed to J.H.

Efficiency enhancement in organic solar cells with ferroelectric polymers

Yongbo Yuan¹, Timothy J. Reece², Pankaj Sharma², Shashi Poddar², Stephen Ducharme^{2,3}, Alexei Gruverman^{2,3}, Yang Yang⁴ and Jinsong Huang^{1,3*}

¹ Department of Mechanical Engineering, University of Nebraska, Lincoln, NE 68588

² Department of Physics and Astronomy, University of Nebraska, Lincoln, NE 68588

³ Nebraska Center for Materials and Nanoscience, Lincoln NE 68583

⁴ Department of Materials Science and Engineering, University of California- Los Angeles, Los Angeles, CA 90095

* To whom correspondence should be addressed: jhuang2@unl.edu

1. The induced electric field in the organic layer by ferroelectric film

We estimated the electric field in the organic layer induced by the ferroelectric film by using a simple model of a semiconductor (S) layer and ferroelectric (FE) layer inserted between two metal electrodes ($M_1/S/FE/M_2$), as shown in Figure S1. There are polarization charges (with a density of $\pm \sigma_p$) on each surface of the poled ferroelectric film. The negative polarization charges at the FE/ M_2 interface are partially screened by the induced positive charges (with a density of $+\sigma_s$) in the metal. As a result, a net electric field penetrates into the organic layer even under short-circuit conditions, as shown in Figure S1b. Here we consider the short-circuit condition for a $M_1/S/FE/M_2$ junction. Charges can move freely between the electrodes through the external circuit so that the potential of the two electrodes is equal at infinity and the charge density at the M_1/S interface is $-\sigma_s$ due to the charge conservation law. We apply a Thomas-Fermi model for the study of screening charges^{1, 2}. According to this model the electrical potential within metal 1 ($z \leq 0$) and metal 2 ($z \geq L+d$) electrode is given by:

$$\varphi_{(z)} = \begin{cases} \frac{\sigma_s \delta_1 e^{-|z|/\delta_1}}{\epsilon_0}, & z \leq 0 \\ -\frac{\sigma_s \delta_2 e^{-|z-L-d|/\delta_2}}{\epsilon_0}, & z \geq L+d \end{cases} \quad (1)$$

here δ_1 and δ_2 are the Thomas-Fermi screening lengths in the M_1 and M_2 electrodes. The $\varphi_{(z)} \rightarrow 0$ when $z \rightarrow \pm\infty$, which is consistent with the short circuit condition. The potential drop between the M_1/S interface and FE/M_2 interface due to the electric field in the organic and ferroelectric layer is determined by:

$$\varphi_{(0)} - \varphi_{(L+d)} = \frac{d(\sigma_p - \sigma_s)}{\epsilon_0 \epsilon_{FE}} - \frac{L\sigma_s}{\epsilon_0 \epsilon_{Org}} \quad (2)$$

here, ϵ_{FE} and ϵ_{Org} is the relative dielectric constant of ferroelectric layer and organic layer, respectively. The screening charge density can be found by the using of equation (1), (2)

$$\sigma_s = \frac{\epsilon_{Org} d \sigma_p}{\epsilon_{FE}(\delta_1 + \delta_2) + \epsilon_{Org} d + \epsilon_{FE} L} \quad (3)$$

Finally the additional electric field E in the organic layer is:

$$E = \frac{\sigma_s}{\epsilon_0 \epsilon_{Org}} = \frac{d \sigma_p}{\epsilon_0 \epsilon_{FE} L} \quad (4)$$

For an ideal condition, the one monolayer (ML) P(VDF-TrFE) on the organic layer is assumed to be continuous and uniform, with a thickness (d) of 1.7 nm^3 . Meanwhile, the thickness of our P3HT:PCBM layer (L) is about 150 nm , the δ_1 and δ_2 will be less than one angstrom for “good” metals, and is negligible as compared to the thickness of the semiconducting polymer. The relative dielectric constant of P(VDF-TrFE) layer (ϵ_{FE}) is

reported to be around 7.5^4 . The polarization charge density (σ_p) of P(VDF-TrFE) is 100 mC/m^2 . Under this condition, the additional electric field added by the 1~3 ML(s) ferroelectric P(VDF-TrFE) layer in the organic semiconductor layer is found to be 17~51 $\text{V}/\mu\text{m}$.

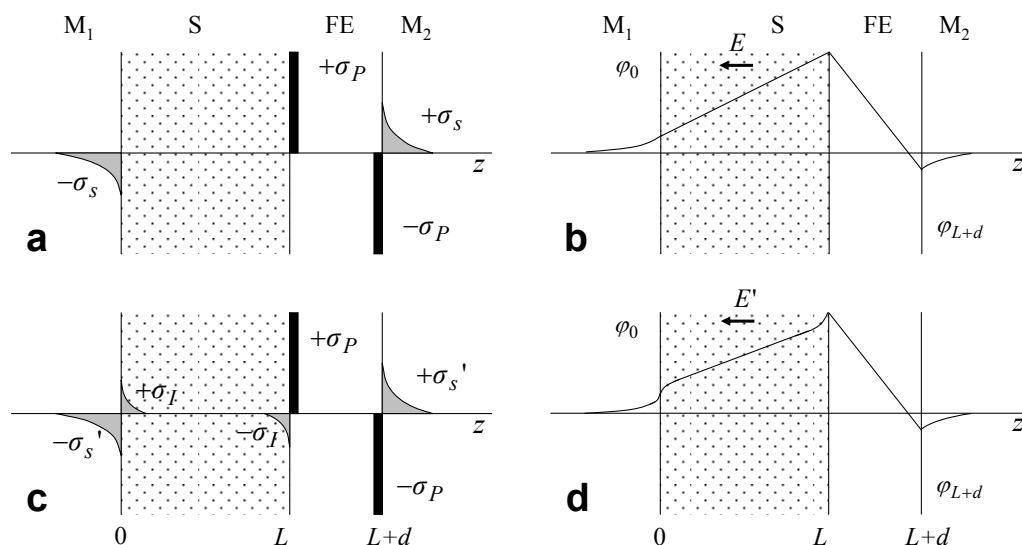


Figure S1. Electrostatics of a $M_1/S/FE/M_2$ junction. **a**, and **c**, Charge distribution, **b**, and **d**, the respective electrostatic potential profile. The polarization charge density at the ferroelectric layer is σ_p , the induced screening charge density at the two electrodes is σ_s or σ_s' , the trapped charges or/and mobile ions accumulated at the M_1/S interface and S/FE interface is σ_I .

The main concern is the possible buildup of electric charge in the cell under solar illumination. If this “space charge density” is too large, then the electric field across the cell will “collapse.” We start with determining the transport time (t_T) of an electron through the semiconductor layer under short-circuit conditions: $L(t) = \mu_e E t_T$, where $L(t)$

is the semiconductor layer thickness, μ_e is an electron mobility. For a better comparison, we used the extracted average electric field E of 12 V/ μm here, which is the electric field estimated from the actual performance of ferroelectric organic photovoltaic (FE-OPV) device as discussed below. We used this transport time to roughly estimate how much the total charge of electrons builds up under solar illumination. We write $\zeta = Jt_T/2$, where ζ is the total electron space charge in the polymer layer (per unit area of the cell). The factor of 2 implies that the current is contributed equally by electrons and holes. For short-circuit conditions with $J_{\text{SC}} = 10 \text{ mA/cm}^2$, we obtain $\zeta = 1.3 \times 10^{-5} \text{ C/m}^2$, which is several orders magnitude less than the polarization charge density of 0.1 C/m^2 at the ferroelectric layer surface. So the photogenerated mobile charges have negligible impact on the induced electric field by the ferroelectric layer. A more sophisticated model is constructed by considering the trapped charges or mobile ions at the S/FE and M₁/S interface, as schemed in Figure S1c. For the first glance, the net electric field in the semiconductor layer will be reduced and the influence of the poled FE layer to the semiconductor layer will be weakened. However, our calculation shows that, in practice, the trapped carriers or/and ions will be screened by the two metal electrodes and the electric field in the organic layer will remain unchanged. The detail calculation is as follows:

$$\varphi_{(z)} = \begin{cases} \frac{\sigma_S' \delta_1 e^{-|z|/\delta_1}}{\epsilon_0}, & z \leq 0 \\ \frac{\sigma_S' \delta_1}{\epsilon_0} + \frac{\sigma_S'}{\epsilon_0 \epsilon_{\text{Org}}} x + \varphi_{I(z)}, & 0 \leq z \leq L \\ -\frac{\sigma_S' \delta_2 e^{-|z-L-d|/\delta_2}}{\epsilon_0}, & z \geq L+d \end{cases} \quad (5)$$

Where the potential $\varphi_{I(z)}$ is the potential distribution contributed by the trapped charges and ions, if present. By assuming the distribution of carriers or/and ions is exponential with a decay length of δ_3 ($\delta_3 \ll L$), the potential $\varphi_{I(z)}$ can be described by Poisson's equation:

$$\frac{d^2 \varphi_{I(z)}}{dz^2} = -\frac{\sigma_I}{\epsilon_0 \epsilon_{Org} \delta_3} (e^{-z/\delta_3} - e^{z-L/\delta_3}) . \quad (6)$$

And similarly, the potential drop across the FE layer should satisfy boundary condition:

$$\varphi_{(L)} - \varphi_{(L+d)} = \frac{(\sigma_P - \sigma_S')d}{\epsilon_0 \epsilon_{FE}} . \quad (7)$$

Using the equation (5), (6) and (7), we arrived at the following value for the screening charge density:

$$\sigma_S' = \frac{\epsilon_{Org} d}{\epsilon_{FE}(\delta_1 + \delta_2) + \epsilon_{FE} L + \epsilon_{Org} d} \sigma_P + \frac{\epsilon_{FE}(L - 2\delta_3)}{\epsilon_{FE}(\delta_1 + \delta_2) + \epsilon_{FE} L + \epsilon_{Org} d} \sigma_I \approx \sigma_S + \sigma_I . \quad (8)$$

By comparing equation (8) with (6), it can be found that the screening charge density at the electrode increased when the trapped charges or mobile ions were accounted. The second item in the right side of equation (8) is induced by the trap charges or/and mobile ions. It approaches to σ_I because the $\epsilon_{FE} L$ is much larger than $\epsilon_{Org} d$, which means most of the trapped carriers or/and mobile ions will be screened by the electrode by add the same amount of charges in the electrode. As a result, after accounting on the space charge in the semiconductor (Figure S1c), the electric field induced in semiconductor layer is nearly unchanged from the situation excluding charge layers within the semiconductor (Figure S1a).

$$E' = \frac{\sigma_S' - \sigma_I}{\epsilon_0 \epsilon_{Org}} \approx E \quad (9)$$

This approximation is a good one because the charge density induced in the semiconductor σ_i is generally much less than σ_p because the extremely low free carrier density in organic semiconductor materials. (In the case of inorganic semiconductors, the free charge density are much larger and therefore the approximation of equation (9) is not so good⁵) This argument is supported by the capacitor measurements which show that the contribution of screening charge to the capacitance of the diodes at reverse bias is effectively negligible.

2. The poling process of devices with ferroelectric layers

For a better understanding of the poling process of the P(VDF-TrFE) layer in the FE-OPV device, we recorded the open circuit voltage (V_{oc}) of device with 1 ML P(VDF-TrFE) under different poling time and temperature condition. The structure of P3HT based FE-OPV device was ITO/PEDOT (30 nm)/P3HT:PCBM (1:1 by wt, 150 nm)/P(VDF-TrFE) (1 ML)/Al. As shown in Figure S2, when a bias of 15 V was applied continuously to the Al electrode at room temperature, the V_{oc} of devices increased slowly, it takes about one hour for the V_{oc} increased from 0.476 V to 0.531 V, demonstrating different degree of partial polarization. While for the device that was poled under 15 V at an elevated temperature of 120 °C for about 15 s and then field-cooled, the V_{oc} increased from 0.474 V to 0.570 V. Heating induces a rapid and more complete poling of P(VDF-TrFE) layer. The switching time of the ferroelectric layer is believed to be limited by the thermal diffusion process because the intrinsic switching time of P(VDF-TrFE) layer is reported to be as short as 100 ns⁶. Accordingly, the poling of devices under -2 V at both heating and field cooling process is referred as negative poling. We use a low bias of -2 V

applied on Al electrode for the negative poling because a higher voltage would induce too much charge injection from ITO/PEDOT:PSS, which burns the devices.

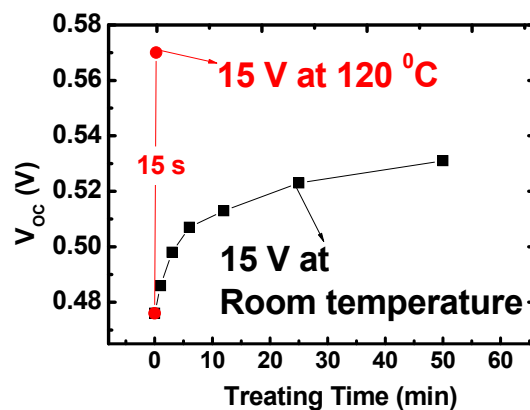


Figure S2. Polarization dynamic process of ferroelectric polymer film in the OPV device.

3. The morphology of P(VDF-TrFE) layers

The morphology of the 0-3 ML(s) of P(VDF-TrFE) LB film on P3HT:PCBM was studied by atomic force microscope (AFM) in tapping mode. The film roughness data are summarized in Table S1. The coating of ferroelectric polymer smoothed the semiconductor films. After annealing, the films become even more smoother. However, as shown in Figure S3, the 3 MLs P(VDF-TrFE) coated on P3HT:PCBM layer aggregates during thermal annealing and forms many nanomesas with a thickness of around 10 nm.⁷ The aggregation of P(VDF-TrFE) may derive from the mismatch of surface energy between P3HT:PCBM film and P(VDF-TrFE) film and the formation of nanomesas helps to minimize the surface energy.⁸

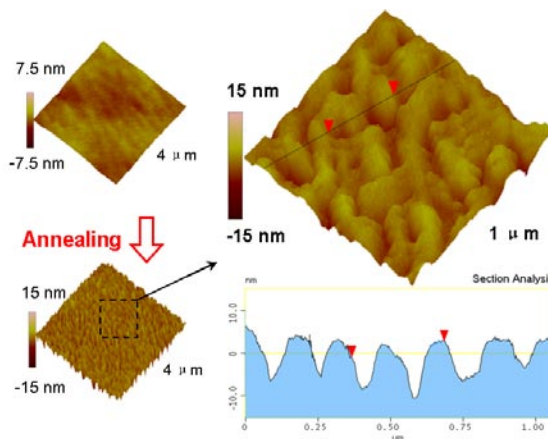


Figure S3. AFM pictures of 3 MLs of P(VDF-TrFE) films on P3HT:PCBM

Table S1. Summary of the roughness of the samples with different monolayer(s) of P(VDF-TrFE) on P3HT:PCBM, before and after annealing.

(PVDF-TrFE)		0 ML	1 ML	2 MLs	3 MLs
RMS	<u>Before Annealing</u>	1.72	1.14	1.25	0.79
(nm)	<u>After Annealing</u>	1.54	1.16	0.98	3.59

4. Effect of the induced field on the photogenerated current of devices.

The photogenerated current of OPV devices obtained by subtracting the dark current from the current under illumination is depend on the effective built-in electric field. The photogenerated current increases linearly near the open-circuit voltage ($V_{oc}-V < 0.1$ V) and saturates at large reverse voltage ($V_{oc}-V > 10$ V). Figure S4 compared the photogenerated current of positively poled FE-OPV and corresponding regular devices. The structures of the regular devices are ITO/PEDOT (30 nm)/P3HT:PC₇₀BM (1:1 by wt, 150 nm)/Al and ITO/PEDOT (30 nm)/PSBTBT:PC₇₀BM (1.5:1 by wt, 90 nm)/Al, respectively. For the FE-OPVs, 1 ML P(VDF-TrFE) was inserted at the cathode interface. The photogenerated current of FE-OPV device at an applied voltage of 0 V (J_{sc}) is equal

to the extrapolated photocurrent of the regular device at an applied voltage of -2.3 V in P3HT:PC₇₀BM device, and 0.8 V in PSBTBT:PCBM device. We simply attribute the increased J_{sc} in FE-OPVs to the electric field induced by the P(VDF-TrFE) layer. Then the induced electric field is roughly estimated by dividing the equivalent applied voltage by the thickness of the semiconductor film, which is approximately 12 ± 3 V/ μm (15 V/ μm in P3HT:PC₇₀BM device, and 9 V/ μm in PSBTBT:PC₇₀BM device).

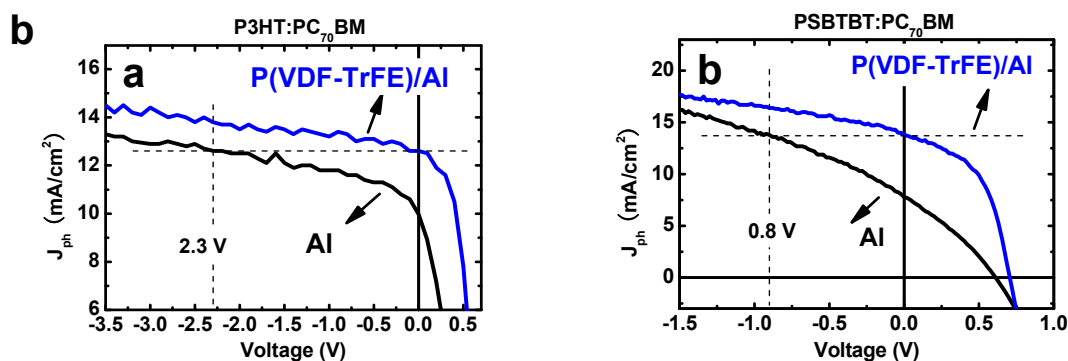


Figure S4 The photogenerated current of positive poled FE-OPV with P(VDF-TrFE)/Al cathode and regular device with Al cathode. The applied voltage across the semiconductor induced by the FE layer is extrapolated.

5. Switching behaviors of the FE-OPVs

The performance of FE-OPV devices can switch between two states repeatedly. Figure S5 show the current density-voltage (I-V) curve of OPV devices with 1 ML P(VDF-TrFE). The J_{sc} of the devices switched between 11.3 ± 0.3 mA/cm² and 7.7 ± 0.6 mA/cm² after alternant positive poling and negative poling. Meanwhile the V_{oc} and fill factor (FF) also switched evidently. After each cycle, all the output parameter came back to same levels. The repeatable switch behaviors of the devices clearly exclude the contributions of annealing effect which may

be proposed to explain the performance improvement observed here⁹.

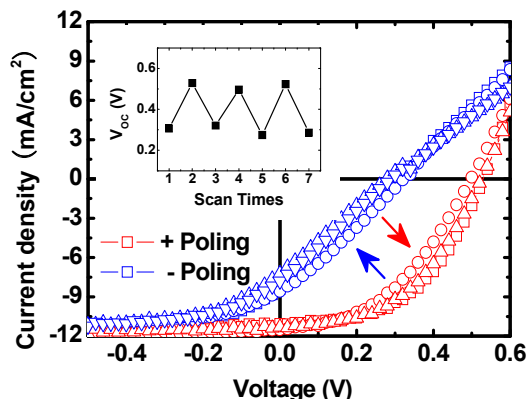


Figure S5 Switching behaviors of OPV device with 1 ML of P(VDF-TrFE) at the cathode interface

For comparison, devices without ferroelectric layer were treated under the same poling condition as the positive poling process. The performance of the devices did not show any visible improvement after poling, as shown in Figure S6. The I-V curve of the poled device was almost identical to that of unpoled device. The results exclude the contribution of other factors, such as ions movement or annealing effects⁹, to the efficiency improvement in FE-OPV devices.

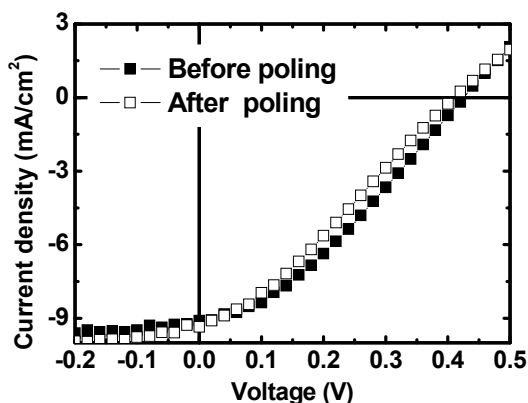


Figure S6. I-V curves of fresh regular OPV devices and the devices after positive poling.

6. P(VDF-TrFE) layer on ITO

In an inverted OPV device using ITO as cathode, the insertion of P(VDF-TrFE) layer also lead to improved device performance and switchable behaviors. The structure of the inverted devices is ITO/P3HT:PCBM (1:1 by wt, 150 nm)/MoO₃ (4 nm)/Ag has an V_{oc} of about 0.18 V. A positive poling of the thin P(VDF-TrFE) layer led to an improved output, and a succedent negative poling process make the performance switching back to a lower level, as shown in Figure S7, and summarized in Table S2. The results demonstrated the switching behaviors are general and independent on the electrode material used.

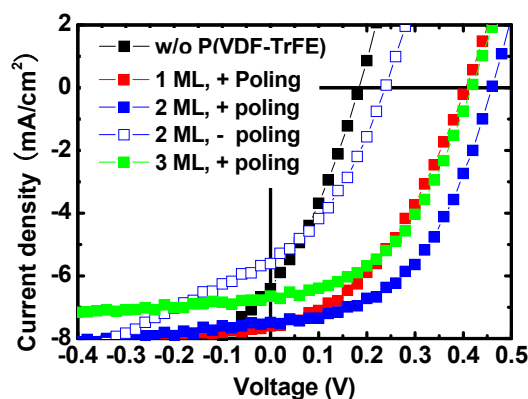


Figure S7. I-V curves of regular invert OPV devices and invert FE-OPV devices with 1-3 ML(s) of P(VDF-TrFE) on the ITO cathode.

Reference

- S1. Ashcroft, N. W. & Mermin, N. D. *Solid State Physics* (Saunders College Publishing, New York, 1976).
- S2. Zhuravlev, M. Y., Sabirianov, R. F., Jaswal, S. S. & Tsymbal, E. Y. Giant electroresistance in ferroelectric tunnel junctions. *Phys.Rev. Lett.* **94**, 246802 (2005).
- S3. Bai, M. & Ducharme, S. Ferroelectric nanomesa formation from polymer Langmuir-Blodgett films. *Appl. Phys. Lett.* **85**, 3528-3530 (2004).
- S4. Ducharme, S., Palto, S. P., Blinov, L. M. & Fridkin, V. M. Physics of two-dimensional ferroelectric polymers. *AIP Conference Proceedings* **535**, 354-363 (2000).
- S5. Reece, T. J. & Ducharme, S. Modeling of metal-ferroelectric-insulator-semiconductor structures based on Langmuir–Blodgett copolymer films. *J. Appl. Phys.* **106**, 124505 (2009).
- S6. Ducharme, S. et al. Intrinsic ferroelectric coercive field. *Phys. Rev. Letts.* **84**, 175-178 (1999).
- S7. Bai, M. et al. Determination of the optical dispersion in ferroelectric vinylidene fluoride (70%)/trifluoroethylene (30%) copolymer Langmuir–Blodgett films. *J. Appl. Phys.* **95**, 3372-3377 (2004).
- S8. Li, J., Luo, Y., Bai, M. & Ducharme, S. A continuum model on the nanomesa and nanowell formation in Langmuir-Blodgett ferroelectric polymeric films. *J. Mech. Phys. Solids* **54**, 2162-2182 (2006).
- S9. Padinger, F., Ritterger, R. S. & Sariciftci, N. S. Effect of postproduction treatment on plastic solar cells. *Adv. Funct. Mater.* **13**, 85-88 (2003).